# Unprecedented Application of Flexible Bis(pyridyl-tetrazole) Ligands To Construct Helix/Loop Subunits To Modify Polyoxometalate Anions

Xiu-Li Wang,* Na Li, Ai-Xiang Tian, Jun Ying, Tian-Jiao Li, Xiao-Ling Lin, Jian Luan, and Yang Yang

Department of Chemistry, Bohai University and Liaoning Province Silicon Materials Engineering Technology Research Centre, Jinzhou 121000, P. R. China

Ⓢ Supporting Information

ABSTRACT: By introducing the unprecedented and flexible isomeric bis(pyridyl-tetrazole) ligands into a polyoxometalates (POMs) system, three POM-based compounds, $\{Ag_2(4\text{-bptzb})_2(H_2O)_2[H_2PMo_{12}O_{40}]_2\}\cdot4\text{-bptzb}\cdot 5H_2O$ (**1**), $[Ag_4(3\text{-bptzb})_2(PMo^VMo^{VI}_{11}O_{40})]\cdot2H_2O$ (**2**), and $Ag_3(3\text{-bptzb})_{2.5}(H_2O)_2[H_3P_2W_{18}O_{62}]$ (**3**) [4-bptzb = 1,4-bis(5-(4-pyridyl)tetrazolyl)-butane and 3-bptzb =1,4-bis(5-(3-pyridyl)tetrazolyl)butane], were synthesized under hydrothermal conditions and structurally characterized by single-crystal X-ray diffraction analyses. Compound **1** exhibits a dimeric structure constructed from two Keggin $[PMo_{12}O_{40}]^{3-}$ anions and a binuclear $[Ag_2(trans\text{-}4\text{-bptzb})_2]^{2+}$ subunit in which the *trans*-4-bptzb acts as a bidentate bridging ligand with one tetrazolyl group. In **2**, the 3-bptzb acts as a tetradentate bridging ligand with the tetrazolyl and pyridyl groups linking Ag^I ions to generate a 3D metal−organic framework (MOF), which contains charming *meso*-helix chains. The Keggin anions acting as bidentate inorganic ligands reside in the distorted tetragonal channels of the MOF. In compound **3**, the 3-bptzb adopts versatile coordination modes linking Ag^I ions to first construct loop connecting loop 1D chains, which are linked by $\{Ag[P_2W_{18}O_{62}]\}_n$ zigzag chains to form a scarce hamburger-style 2D sheet. These adjacent sheets are further fused by 3-bptzb ligands to construct a 3D framework. The influences of isomeric bptzb ligands and POMs on the construction of Ag-bptzb subunits and the whole structures of the title compounds are discussed. The electrochemical behaviors and electrocatalytic activities of compounds **2** and **3** and their corresponding parent POMs as well as the fluorescent properties of the title compounds have been studied in detail. In addition, the photocatalytic activities of compounds **2** and **3** and their corresponding parent POMs for decomposition of methylene blue, rhodamine B, and methyl orange under UV irradiation have also been investigated.
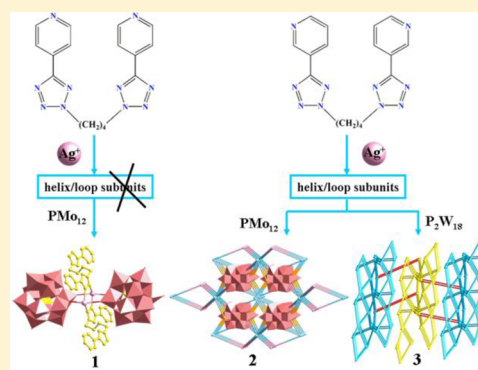
■ INTRODUCTION

Over the last decades, design and synthesis of metal−organic complexes (MOCs) have aroused considerable attention, arising not only from their potential applications in many areas[1] but also as a result of their chemical and structural diversities.[2] Recently, utilization of secondary building units (SBUs) for constructing MOCs materials with charming configurations and desired properties represents a remarkable branch.[3] Polyoxometalates (POMs) have been regarded as one kind of structurally outstanding SBUs due to their coordination ability, structural diversity, and promising properties, such as catalytic activity, magnetism, photochemical activity, electrochemical activity, and so on.[4] Therefore, introduction of POMs to MOCs is a rational approach for constructing POMs-based MOCs materials, which may incorporate the merits of both components.[5]

To date, lots of POM-based MOCs have been reported in which the POMs usually act as noncoordinated anionic templates or multidentate inorganic ligands.[6] Among these POM-based MOCs, the examples on assembly of combining POMs and helix/loop metal−organic subunits are still relatively limited. Moreover, most of the POM-based helix/loop structures are discrete structures or low-dimensional networks.[7,8] Thus, rational design and assembly of high-dimensional POM-based MOCs from helix/loop subunits is still an appealing and a challenging work.

As is known, many factors could influence the assembly process of POM-based MOCs, for instance, the type of POM anions, the coordination geometry of metal ions, the nature of organic ligands, and the topological and geometrical relations of both the metal ions and the ligands.[9] Compared with other factors, design of proper organic ligands is crucial for construction of helix/loop subunits for modification of POMs, including length, geometry, coordination ability, and relative orientation of the donor groups.[10] According to the reported helix/loop structures, we noticed the following. (i) It is difficult to obtain high-dimensional structures with helix/loop subunits using some rigid ligands. (ii) The organic ligand has side coordination donors usually conducive to forming helix/

loop structures. For instance, Long's group used the 2,4′-bipy ligand to construct five Keggin-based MOCs, which possess different cyclic structures.[11] (iii) The flexible polydentate ligands especially containing $-(CH_2)_n-$ backbones may induce the helix/loop subunits with ease owing to their flexibility and conformational freedom, which can make them conform to the coordination environment of the metal ions and POMs.

In our previous work, we successfully designed a series of rigid triazole/tetrazole-based ligands, introduced them to POM−Cu^I/Ag^I systems, and obtained some novel POM-based multinuclear clusters.[12] In this work, we try to improve the rigid pyridyl-tetrazole precursors (4-ptzH and 3-ptzH, Scheme S1, Supporting Information) via introducing flexible $-(CH_2)_4-$ backbones, aiming to construct helix/loop subunits in POMs system. As a result, two isomeric flexible bis(pyridyl-tetrazole) ligands 1,4-bis(5-(4-pyridyl)tetrazolyl)butane (4-bptzb) and 1,4-bis(5-(3-pyridyl)tetrazolyl)butane (3-bptzb) were first designed and obtained (Schemes 1 and S1,

Scheme 1. Main Coordination Modes of the Bis(Pyridyl-tetrazole) Ligands (4-bptzb and 3-bptzb) in This Work
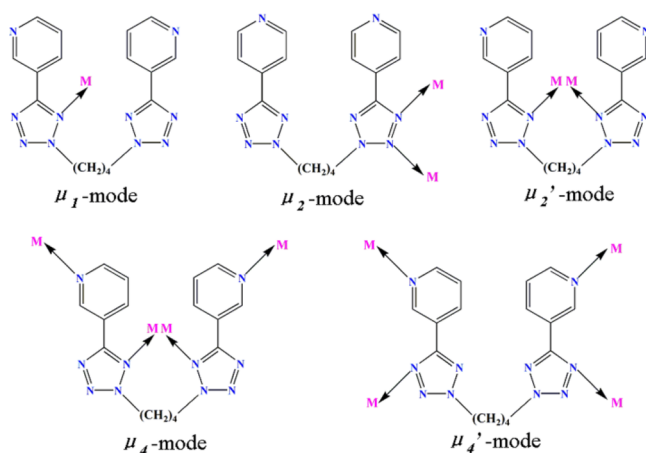
Supporting Information). These two flexible bis(pyridyl-tetrazole) ligands possess distinctive advantages: (i) they can provide multiple coordination sites including side N donors

and form versatile coordination modes; (ii) they have pyridyl groups for expanding the dimensionality and obtaining new attractive frameworks; (iii) these ligands have flexible $-(CH_2)_4-$ backbones. Importantly, to the best of our knowledge, research on the bis(pyridyl-tetrazole) ligands in POMs system or coordination compounds has not been reported to date. We want to verify whether our improved synthetic strategy is rational for construction of helix/loop structures in POMs system, which may also offer informative examples for target syntheses and develop new synthetic routes as well.

Fortunately, three new POM-based MOCs were obtained, $\{Ag_2(4\text{-bptzb})_2(H_2O)_2[H_2PMo_{12}O_{40}]_2\}\cdot4\text{-bptzb}\cdot5H_2O$ (**1**), $[Ag_4(3\text{-bptzb})_2(PMo^VMo^{VI}_{11}O_{40})]\cdot2H_2O$ (**2**), and $Ag_3(3\text{-bptzb})_{2.5}(H_2O)_2[H_3P_2W_{18}O_{62}]$ (**3**). Among these compounds, **2** and **3** contain helix/loop subunits as expected. Scheme 1 summarizes the coordination modes of these bis(pyridyl-tetrazole) ligands in this paper. The influences of isomeric ligands and POMs on construction of Ag−bptzb subunits and the whole structures were discussed. The electrochemical and photocatalytic properties of compounds **2** and **3** and their corresponding parent POMs as well as the fluorescent properties of the title compounds have also been investigated.

■ EXPERIMENTAL SECTION

Materials and Methods. All reagents and solvents for syntheses were purchased from commercial sources and used as received without further purification.

Physical Measurements. Elemental analyses (C, H, N) were carried out with a PerkinElmer 240C elemental analyzer. Inductively coupled plasma (ICP) analyses were performed on a VISTA-MPX ICP-OES spectrometer. FT-IR spectra were taken on a Varian 640-IR spectrometer (KBr pellets). Powder XRD investigations were carried out with an Ultima IV with D/teX Ultra diffractometer at 40 kV, 40 mA with Cu Kα radiation. Thermal gravimetric analyses (TGA) were carried out in N$_2$ on a Pyris-Diamond thermal analyzer with a rate of 10 °C min^{-1}. Electrochemical measurements and data collection were performed with a CHI 440 electrochemical workstation connected to a Digital-586 personal computer. A conventional three-electrode system was used with a saturated calomel electrode (SCE) as the reference electrode and a Pt wire as the counter electrode. The title compound bulk-modified carbon paste electrodes (CPEs) were used as the working electrodes. UV−vis absorption spectra were obtained using a

Table 1. Crystallographic Data for Compounds 1−3

compounds	1	2	3
formula	$C_{48}H_{66}Ag_2Mo_{24}N_{30}O_{87}P_2$	$C_{32}H_{36}Ag_4Mo_{12}N_{20}O_{42}P$	$C_{40}H_{47}Ag_3W_{18}N_{25}O_{64}P_2$
fw	5035.55	2986.54	5596.88
crystasyst	triclinic	monoclinic	monoclinic
space group	$P\bar{1}$	$C2/c$	$P2_1/c$
a (Å)	12.2188(8)	21.7793(15)	28.0496(19)
b (Å)	13.7977(10)	24.0089(15)	15.2674(10)
c (Å)	19.6975(13)	13.1613(8)	22.9741(15)
α (deg)	70.6480(10)	90	90
β (deg)	75.6910(10)	99.0040(10)	99.0030(10)
γ (deg)	69.1690(10)	90	90
V (Å^3)	2896.7(3)	6797.2(8)	9717.3(11)
Z	1	4	4
D_c (g cm^{-3})	2.882	2.918	3.821
GOF	1.012	1.041	1.038
$R_1{}^a[I > 2\mathrm{sigma}(I)]$	0.0346	0.0530	0.0698
$wR_2{}^b$ (all data)	0.0853	0.1659	0.1839

$^a R_1 = \sum ||F_0| - |F_c|| / \sum |F_0|$. $^b wR_2 = \{\sum[w(F_0^2 - F_c^2)^2]/\sum[w(F_0^2)^2]\}^{1/2}$.

SP-1900 UV/vis spectrophotometer. XPS analyses were carried out with a Thermo SCIENTIFIC ESCALAB 250. Fluorescence spectra were recorded on a Hitachi F-4500 fluorescence/phosphorescence spectrophotometer.

X-ray Crystallography. Crystallographic data for compounds **1**–**3** were collected on a Bruker SMART APEX II with Mo Kα (λ = 0.71073 Å) by ω and θ scan mode. All structures were solved by direct methods and refined on F^2 by full-matrix least-squares using the SHELXL package.[13] In order to subtract the contribution of the disordered solvent molecules in compound **3**, the SQUEEZE command was applied. SQUEEZE removed three H_2O for **3**. This value is calculated based upon volume/count_electrons analysis and the TG data of compound **3**. For compounds **1** and **3**, some hydrogen atoms attached to water molecules were not located but included in the structure factor calculations. For **2**, all hydrogen atoms attached to water molecules were located. Detailed crystal data and structure refinement for **1**–**3** are given in Table 1. Selected bond lengths and angles are listed in Table S1, Supporting Information. Crystallographic data for the structures reported in this paper have been deposited in the Cambridge Crystallographic Data Center with CCDC Numbers 998452−998454.

Preparation of Compounds 1–3. Synthesis of {Ag₂(4-bptzb)₂(H₂O)₂[H₂PMo₁₂O₄₀]₂}·4-bptzb·5H₂O (1). A mixture of $AgNO_3$ (0.08 g, 0.47 mmol), 4-bptzb (0.015 g, 0.05 mmol), and $H_3PMo_{12}O_{40}$ (0.1 g, 0.05 mmol) was dissolved in 10 mL of distilled water at room temperature. The suspension was stirred for about 1 h, and the pH value was then adjusted to about 1.16 using 1.0 mol·L^{-1} HNO_3. The suspension was transferred to a Teflon-lined autoclave (25 mL) and kept at 160 °C for 4 days. After slow cooling to room temperature (final pH = 1.30), yellow block crystals of **1** were obtained. Yield 62% based on Mo. Anal. Calcd for $C_{48}H_{66}Ag_2N_{30}O_{87}P_2Mo_{24}$ (5035.55): C, 11.43; H, 1.31; N, 8.34; P, 1.23; Mo, 45.73; Ag, 4.28. Found: C, 11.38; H, 1.29; N, 8.28; P, 1.18; Mo, 45.65; Ag, 4.21. IR (KBr pellet, cm^{-1}): 3497 (w), 3103 (w), 2357 (m), 1645 (s), 1605 (w), 1569 (w), 1516 (w), 1459 (w), 1404 (w), 1243 (w), 1208 (w), 1063 (s), 959 (s), 877 (m), 801 (s), 607 (w).

Synthesis of [Ag₄(3-bptzb)₂(PMoᵛMoᵛᴵ₁₁O₄₀)]·2H₂O (2). The synthetic method was similar to that of compound **1**, except that 3-bptzb (0.015 g, 0.05 mmol) was used instead of 4-bptzb and the pH value was adjusted to about 1.68. Yellow block crystals of **2** were obtained (final pH = 2.10). Yield 58% based on Mo. Anal. Calcd for $C_{32}H_{36}Ag_4N_{20}O_{42}PMo_{12}$ (2986.54): C, 12.86; H, 1.21; N, 9.38; P, 1.04; Mo, 38.55; Ag, 14.45. Found: C, 12.80; H, 1.19; Mo, 38.63; Ag, 14.50. IR (KBr pellet, cm^{-1}): 3518 (w), 2362 (m), 1619 (m), 1561 (w), 1451 (w), 1424 (m), 1386 (w), 1201 (w), 1161 (w), 1138 (w), 1058 (s), 957 (s), 872 (s), 799 (s), 687 (m), 506 (w).

Synthesis of Ag₃(3-bptzb)₂.₅(H₂O)₂[H₃P₂W₁₈O₆₂] (3). A mixture of $AgNO_3$ (0.08 g, 0.47 mmol), 3-bptzb (0.015 g, 0.05 mmol), α-$K_6P_2W_{18}O_{62}$·15H$_2$O (0.1 g, 0.021 mmol), and NH_4VO_3 (0.012 g, 0.1 mmol) was dissolved in 10 mL of distilled water at room temperature. The pH of the mixture was adjusted to about 0.6 with 1.0 mol·L^{-1} HNO_3. The mixture was stirred for about 1 h, transferred to a 25 mL Telfon reactor, and then heated at 160 °C for 8 days. After slow cooling to room temperature (final pH = 1.01), pale yellow block crystals of **3** were obtained. Yield 45% based on W. Anal. Calcd for $C_{40}H_{47}Ag_3N_{25}O_{64}P_2W_{18}$ (5596.88): C, 8.58; H, 0.84; N, 6.25; P, 1.11; Ag, 5.78; W, 59.13. Found: C, 8.53; H, 0.81; N, 6.25; P, 1.08; Ag, 5.76; W, 59.10. IR (KBr pellet, cm^{-1}): 3490 (w), 2362 (m), 1642 (m), 1611 (w), 1584 (w), 1497 (w), 1466 (m), 1363 (w), 1261 (w), 1198 (w), 1095 (s), 957 (s), 912 (s), 789 (s), 674 (m), 529 (m).

Preparation of Compounds 2 and 3 Bulk-Modified CPEs. Compound **2** bulk-modified CPE (**2**−CPE) was obtained as follows:[14] the graphite powder (0.10 g) and compound **2** (0.01 g) were mixed and ground together by agate mortar and pestle for approximately 30 min to achieve the dry mixture. Then the paraffin oil (0.15 mL) was added and stirred with a glass rod. The homogenized mixture was enclosed to 3 mm inner diameter glass tubes to a length of 0.8 cm. The tube surface was wiped with weighing paper, and the electrical contact was established with the copper wire through the back of the electrode. In a similar manner, **3**−CPE was manufactured with compound **3**.

Furthermore, the $Na_3PMo_{12}O_{40}$ and α-$K_6P_2W_{18}O_{62}$·15H$_2$O bulk-modified CPE (PMo_{12}−CPE and P_2W_{18}−CPE) were obtained using a similar method as well.

■ RESULTS AND DISCUSSION

Structural Description. *Ag₂(4-bptzb)₂(H₂O)₂[H₂PMo₁₂-O₄₀]₂}·4-bptzb·5H₂O (1).* X-ray crystal structure analysis reveals that compound **1** is composed of two Ag^I ions, two coordinated 4-bptzb ligands and one discrete 4-bptzb ligand, two $[PMo_{12}O_{40}]^{3-}$ (abbreviated as **PMo₁₂**) anions, and two coordinated and five crystallization water molecules (Figure S1, Supporting Information). In order to balance the charges, two free protons have been added to the molecular formula.[15] Valence sum calculations[16] show that all Mo atoms are in the +VI oxidation state, and all Ag atoms are in the +I oxidation state.

Two distinct motifs could be identified in the structure of compound **1**: a binuclear $[Ag_2(trans\text{-}4\text{-}bptzb)_2]^{2+}$ subunit (I) and a Keggin cluster **PMo₁₂** (II) (Figure 1a). In motif I, Ag1
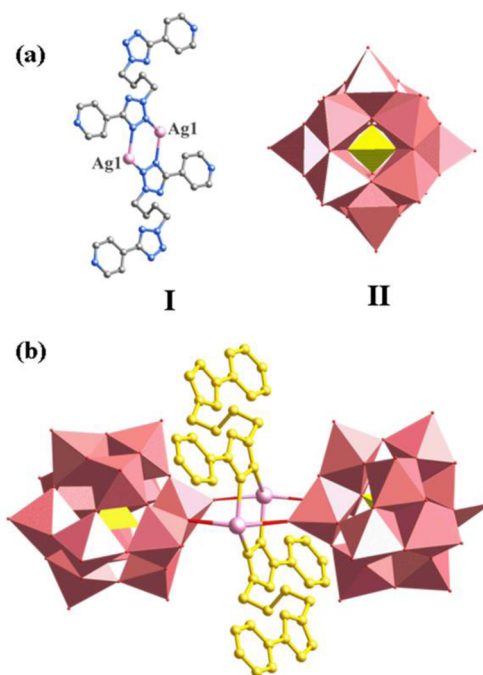
Figure 1. (a) View of the two distinct motifs in **1**: I, [[Ag₂(4-*trans*-bptzb)₂]²⁺ subunit, and II, Keggin cluster PMo₁₂; (b) dimeric structure of **1**. Coordination water molecules have been omitted for clarity.

ion with a distorted trigonal bipyramidal geometry is five coordinated by two N atoms (N9 and N13) from two *trans*-4-bptzb ligands, two O atoms (O28 and O29) from two PMo₁₂ anions, and one water molecule (Figure S1, Supporting Information), with Ag−N bond distances of 2.369(5) and 2.447(5) Å, Ag−O bond distances of 2.313(5)−2.506(4) Å, a N−Ag−N angle of 118.45(17)°, and N−Ag−O angles of 72.23(16)−119.70(18)° (Table S1, Supporting Information). The *trans*-4-bptzb ligand, acting as a bidentate bridging ligand, utilizes two adjacent N donors from one tetrazolyl group to link two Ag^I ions, resulting in a "Z"-type conformation mode (μ_2'-coordination mode), namely, two Ag1 ions are bridged by two "Z"-type conformational 4-bptzb ligands to form a binuclear $[Ag_2(trans\text{-}4\text{-}bptzb)_2]^{2+}$ subunit (Figure 1a). Motif II shows the well-known saturated Keggin anion. P−O and Mo−O lengths

are in the normal ranges.[17] Two PMo$_{12}$ anions providing two terminal oxygen atoms coordinate with two Ag^I ions from motif I, building a dimeric structure (Figure 1b).

Furthermore, detailed structural analysis reveals that these dimers are further connected by O3W via hydrogen-bonding interactions (O(3W)−H(3B)···O(33) = 2.324 Å), forming a 1D supramolecular chain (Figure 2a, Table S2, Supporting
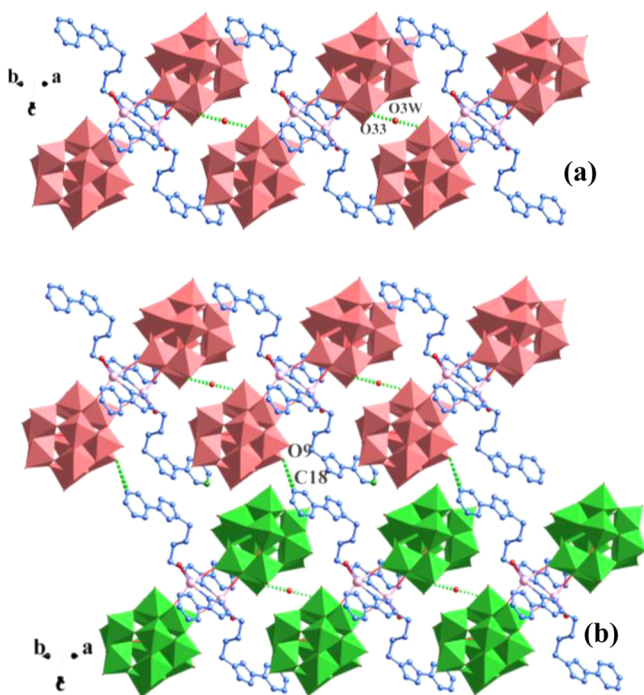
Figure 2. (a) View of the 1D supramolelar chain connected by O3W via hydrogen-bonding interactions (O(3W)−H(3B)···O(33) = 2.324 Å); (b) 2D supramolelar network of **1** with C−H···O hydrogen-bonding interactions (C(18)−H(18A)···O(9) = 3.259 Å).

Information). Adjacent chains are further connected by C−H···O hydrogen-bonding interactions between carbon atoms of 4-bptzb and terminal oxygen atoms of PMo$_{12}$ anions to build a 2D supramolecular network (C(18)−H(18A)···O(9) = 3.259 Å), as shown in Figure 2b. In addition, the 3D supramolecular framework linked by C−H···O (C(17)−H(17A)···O(10) = 3.166 Å) hydrogen-bonding interactions is constructed (Figure S2, Supporting Information).

[Ag$_4$(3-bptzb)$_2$(PMo^{V}Mo$^{VI}_{11}$O$_{40}$)]·2H$_2$O (2). In order to construct the helix subunits and further investigate the influence of the isomeric ligands on the final structure, we employed a 3-bptzb ligand in **2**, which has one side N donor in the pyridyl group. As expected, compound **2** with a *meso*-helix chain was obtained. The asymmetric unit of **2** contains four Ag^I ions, two 3-bptzb ligands (one *trans*-3-bptzb and one *cis*-3-bptzb), one PMo$_{12}$ anion, and two crystalline water molecules (Figure S3, Supporting Information). Valence sum calculations[16] show one Mo atom of each PMo$_{12}$ anion is in the +V oxidation state and all Ag atoms are in the +I oxidation state.

In compound **2** there are two crystallographically independent Ag^I ions (Ag1 and Ag2) which exhibit two types of coordination geometries. (i) The Ag1 ion is two coordinated by two N donors (N5 and N6) from the pyridyl group of two 3-bptzb ligands in a linear geometry {AgN$_2$} with Ag−N distances of 2.139(7) and 2.146(7) Å and a N−Ag−N angle

of 174.0(3)°. (ii) The Ag2 ion shows a three-coordinated configuration {AgN$_2$O}, which is completed by one terminal oxygen atom (O5) from one PMo$_{12}$ anion and two N atoms (N1 and N10) from the tetrazolyl group of two 3-bptzb ligands (Table 2). The bond distances around the Ag2 ion are 2.205(7) and 2.312(7) Å for Ag−N and 2.361(7) Å for Ag−O, while the N−Ag−N angle is 131.1(3)°, and the N−Ag−O angles are 93.7(3)° and 133.5(3)° (Table S1, Supporting Information). These bond distances and angles are comparable to those in the Ag^I compounds.[18] The 3-bptzb ligands in compound **2** show two types of conformation modes: μ_4- and μ_4'-coordination mode (Scheme 1), which both utilize four N donors to link four Ag^I ions, acting as tetradentate bridging ligands.
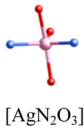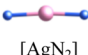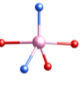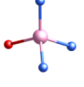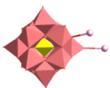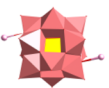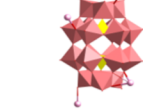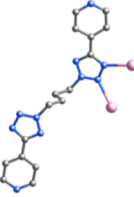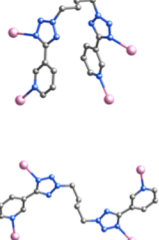
The notable feature of compound **2** rests on the *meso*-helix chain constructed by Ag^I ions and 3-bptzb ligands. The "S"-type and "U"-type 3-bptzb ligands connect with Ag1 ions alternately (Figure 3a), giving a charming *meso*-helix chain [(Ag1)$_4$(3-bptzb)$_2$)]$_n$ with the 1D channel (Figure 3b and 3c). It is noticeable that all Ag^I ions are connected by side N atoms in pyridyl groups of 3-bptzb ligands, namely, this side pyridyl N donor induces formation of the *meso*-helix chain subunit. Formation of *meso*-helix chain [(Ag1)$_4$(3-bptzb)$_2$)]$_n$ in compound **2** just meets our purposes for choosing 3-bptzb ligand and confirms that our synthetic strategy is rational to explore helix subunits.

The adjacent *meso*-helix chains [(Ag1)$_4$(3-bptzb)$_2$)]$_n$ connect with each other through Ag2 ions to construct a 3D metal−organic framework (MOF) (Figure 4a). It is noted that Ag2 ions alternately link tetrazolyl N donors from "S"-type and "U"-type 3-bptzb ligands (Figure S4, Supporting Information). In addition, the 3D MOF contains three kinds of channels (A, B, and C) in which the channel A with dimension of ca. 16.8 × 18.9 Å^2 is large enough to accommodate the nanosized PMo$_{12}$ anion (Figure S5, Supporting Information). Thus, the PMo$_{12}$ anion offers two terminal O atoms to coordinate with two Ag2 ions of the 3D MOF and resides in the "distorted" tetragonal channel A (Figure 4b).
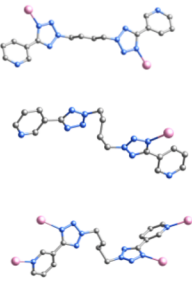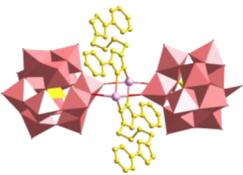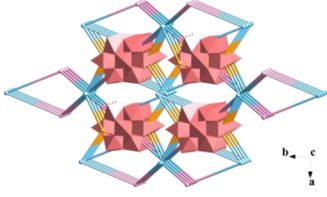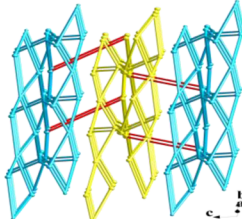
Ag$_3$(3-bptzb)$_{2.5}$(H$_2$O)$_2$[H$_3$P$_2$W$_{18}$O$_{62}$] (3). To further investigate the influence of the anions and obtain the charming structures, we introduced [P$_2$W$_{18}$O$_{62}$]$^{6−}$ (abbreviated to P$_2$W$_{18}$) anions to the Ag/3-bptzb system. Fortunately, compound **3** with loop subunits was obtained. Crystal structure analysis reveals that compound **3** consists of 3 Ag^I ions, 2.5 3-bptzb ligands, 1 Well-Dawson P$_2$W$_{18}$ cluster, and 2 coordinated water molecules (Figure S6, Supporting Information). Valence sum calculations[16] show that all W atoms of the P$_2$W$_{18}$ anion are in the +VI oxidation state and all Ag atoms are in the +I oxidation state. Similar to **1**, to balance the charge of compound **3**, three protons were added in a P$_2$W$_{18}$ anion of the formula.

In compound **3**, there are three crystallographically independent Ag^I ions (Ag1, Ag2, and Ag3) exhibiting three kinds of coordination modes (four-, five-, and six-coordinated modes), which are more multiple than those in **1** and **2**. The Ag1 ion is six coordinated in a distorted octahedral geometry of {Ag(1)NO$_5$} by one N atom from the tetrazolyl group of a 3-bptzb ligand, four O atoms (O11, O37, O46, and O58) from two P$_2$W$_{18}$ anions, and one water molecule. The bond distances and angles are 2.251(16) Å for Ag−N, 2.406(19)−2.710(19) Å for Ag−O, 78.5(6)° for the N−Ag−N angle, and 78.5(6)° and 108.7(7)° for N−Ag−O angles. Ag2 adopts a five-coordination "square pyramid" geometry of {Ag(2)N$_2$O$_3$}, which is coordinated by two N atoms from a pyridyl group of a 3-bptzb ligand and a tetrazolyl group of another 3-bptzb ligand,

Table 2. Coordination Numbers and Modes of POMs, Organic Ligands (4-bptzb and 3-bptzb), Ag^I Ions, and Frameworks of Compounds 1−3

Compounds	1	2	3
The POMs	PMo$_{12}$	PMo$_{12}$	P$_2$W$_{18}$
The ligands	4-bptzb	3-bptzb	3-bptzb
Coordination modes of silver ions	[AgN$_2$O$_3$]	[AgN$_2$] [AgN$_2$O]	[AgNO$_5$] [AgN$_2$O$_3$] [AgN$_3$O]
Coordination sites of polyanions			
Coordination modes and conformations of ligands			
Frameworks			

two O atoms (O26 and O42) from two P$_2$W$_{18}$ clusters, and one water molecule. The bond distances and angles around Ag2 are 2.25 (2) Å for Ag−N, 1.70(2) and 2.419(15) Å for Ag−O, 170.1(8)° for the N−Ag−N angle, and 63.9(8)−121.5(6)° for N−Ag−O angles. The Ag3 ion is four coordinated by three N atoms from two tetrazolyl and one pyridyl groups of three 3-bptzb ligands and one O48 atom from one P$_2$W$_{18}$ cluster with Ag3−N distances of 2.25(2)−2.42(2) Å, a Ag3−O distance of 2.530(14) Å, N−Ag3−N angles of 100.1(8)−119.0(7)°, and N−Ag3−O angles of 92.2(6)−115.6(7)° (Table S1, Supporting Information), exhibiting a "cross" geometry of {Ag(3)N$_3$O}. The 3-bptzb ligands in compound **3** show three types of coordination modes: μ_1, μ_2', and μ_4' modes (Scheme 1). The μ_1 mode of 3-bptzb utilizes one N atom of the tetrazolyl group to link one Ag3 ion (Figure S7, Supporting Information), while the μ_2' mode of 3-bptzb acts as a bidentate bridging ligand using two N atoms of two tetrazole groups to fuse two Ag^I ions. The μ_4'-coordination mode is similar to that in **2** (Table 2).

In compound **3**, two 3-bptzb ligands with μ_4'-mode link two Ag^I ions (Ag2 and Ag3) to form a dinuclear loop with a dimension of ca. 7.16 × 5.37 Å (Figure S8, Supporting

Information). These loops further connect with each other through sharing the same Ag^I ions (Ag2 and Ag3), and a 1D chain with loop connecting loop style is generated (Figure 5a). In summary, the side N donors in both pyridyl and tetrazolyl groups of 3-bptzb ligands lead to formation of the loop structure of **3**. Another structural feature in compound **3** is that each P$_2$W$_{18}$ anion links two Ag1 atoms alternately and each Ag1 atom links two P$_2$W$_{18}$ anions, forming a 1D {Ag[P$_2$W$_{18}$]}$_n$ inorganic zigzag chain in the mode of "hand by hand" (Figure 5b). Each {Ag[P$_2$W$_{18}$]}$_n$ zigzag chain connects with four adjacent 1D loop chains through a Ag−O bond, resulting in a hamburger-style structure (Figures 6a and Figure S9a, Supporting Information), namely, the {Ag[P$_2$W$_{18}$]}$_n$ zigzag chain is sandwiched by two pairs of loop chains. Thus, each P$_2$W$_{18}$ anion offers two terminal O atoms and five bridging O atoms to coordinate with five Ag^I ions, acting as a five-connected inorganic ligand (Figure S10, Supporting Information), which is scarce in POM-based compounds, to the best of our knowledge. Furthermore, the neighboring hamburger-style subunits are linked together by sharing the Ag^I ions in the loops to construct 2D sheets (Figures 6b, 6c, and S9b, Supporting
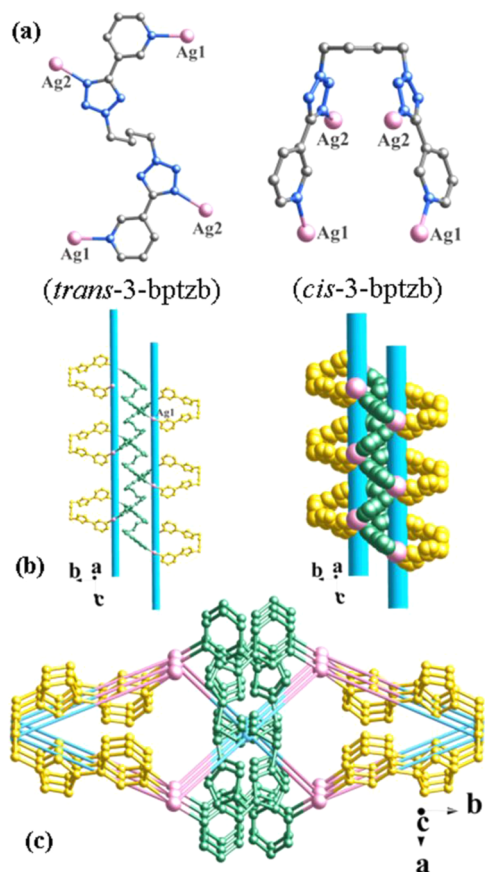
Figure 3. (a) Coordination modes of the "S"-type and "U-type 3-bptzb ligands in **2**; (b and c) *meso*-helix chain $[(Ag1)_4(3\text{-bptzb})_2)]_n$ viewed along the *a* (b) or *c* axis in **2** (c).

Figure 4. (a) Schematic diagram of Ag^I−3-bptzb 3D MOF of **2** with three kinds of channels (A, B, and C); (b) schematic diagram of PMo_{12} anions incorporated into the largest channels A of the 3D MOF.

Figure 5. (a) 1D Ag^I−3-bptzb chain of **3** with loop connecting loop mode; (b) 1D $\{Ag[P_2W_{18}]\}_n$ inorganic zigzag chain in the mode of "hand by hand".

Information). These adjacent 2D sheets are further extended by 3-bptzb ligands with μ_2'-mode into a 3D framework (Figure 7).

Influence of Flexible −(CH₂)₄− Spacer of Bis(pyridyltetrazole) Ligands on Formation of Helix/Loop Subunits. In this work, by introducing the flexible −$(CH_2)_4$− spacer into rigid multidentate tetrazole-based precursors of 4-ptzH and 3-ptzH, we achieved two flexible bis(pyridyltetrazole) ligands aiming to observe the effect of spacer on assembly of helix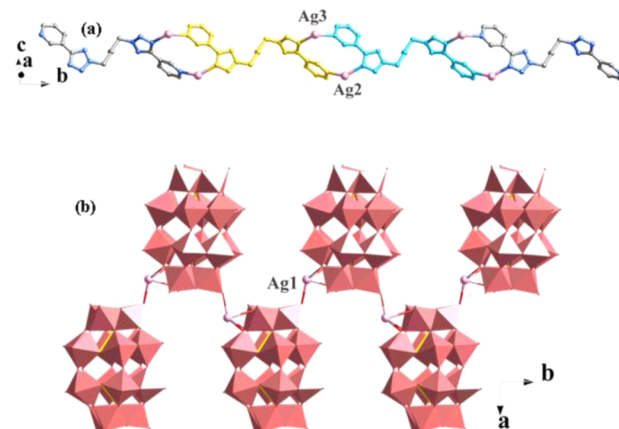/loop subunits in POM-based MOCs. As validated by many research groups, we learned that the rigid tetrazole-based ligands readily induce forming multinuclear subunits.[19] For instance, Yan's group used 2-ptzH, 3-ptzH, and 4-ptzH to construct a series of Keggin- and Dawson-based compounds which possess different multinuclear clusters.[20] Peng's group also reported a series of Keggin-based multinuclear Cu^I subunits using the 2-ptzH ligand.[21] Recently, our group also obtained some multinuclear POM-based compounds using the rigid tetrazole-based ligands.[12] However, in order to construct the helix/loop subunits in POMs system, we inserted the flexible −$(CH_2)_4$− spacer into the rigid 3-ptzH and 4-ptzH ligands and introduced the flexible 3-bptzb and 4-bptzb to Ag/POMs system. Fortunately, compound **2** with helix subunits and compound **3** with loop subunits were obtained with 3-bptzb as expected. Compared with rigid precursors of 4-ptzH and 3-ptzH, the flexible 3-bptzb forms helix/loop subunits instead of multinuclear subunits. This result proves that introducing the −$(CH_2)_4$− spacer into the rigid tetrazole-

based precursors is rational for construction of helix/loop subunits.

Effects of Isomers 4- and 3-bptzb Ligands on Construction of Helix/Loop Subunits and the Final Structures. According to many reports on POM-based MOCs, we noticed that the organic ligands have side coordination donors conducive to forming helix/loop structures, such as 2,4'-bipy,[11,22] whereas those with apical coordination donors usually induce multitrack or linear metal−organic subunits, such as 4,4'-bipy.[23] Moreover, introduction of a flexible spacer to the organic ligands with side donors is more favorable to build helix/loop subunits.[24] In this work, we used 4-bptzb to construct POM-based MOCs first. The 4-bptzb owns one
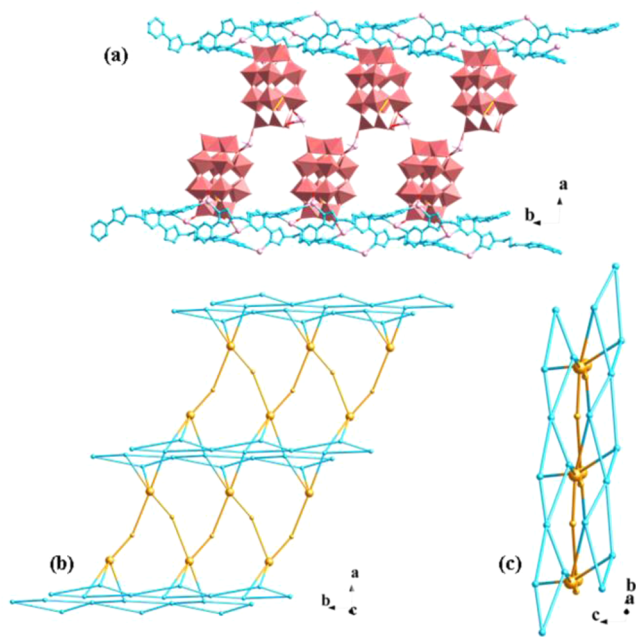
Figure 6. (a) Hamburger-style subunit constructed from a {Ag-[P_2W_{18}]}$_n$ zigzag chain and four 1D loop chains in compound **3**; (b and c) schematic view of the 2D sheets based on the hamburger-style structure along the c (b) or a axis (c).
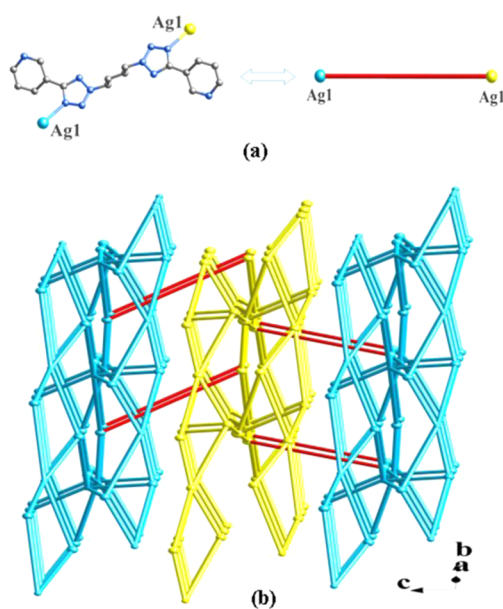
Figure 7. (a) 3-bptzb ligand as a linkage; (b) schematic diagram of the 3D framework (red line, 3-bptzb ligands for linking two adjacent 2D layers).

tetrazolyl group containing side N donors, while the N donor in the pyridyl group rests on the apical site. We want to explore whether the side N donors of the tetrazolyl group can induce formation of helix/loop structures. However, in compound **1**, the 4-bptzb acts a bidentate bridging ligand with two adjacent N atoms from one tetrazolyl group linking two Ag^I ions, forming a binuclear [Ag$_2$(*trans*-4-bptzb)$_2$]$^{2+}$ subunit, with no helix/loop feature. Two Keggin PMo$_{12}$ anions coordinate with the [Ag$_2$(*trans*-4-bptzb)$_2$]$^{2+}$ subunit; thus, a Keggin-based dimer was obtained. It is inferred that the N donor site in the pyridyl

group may play the key role in construction of helix/loop structures. Thus, we change our synthetic strategy by tuning the N sites in the pyridyl group and the 3-bptzb ligand was employed in **2**. As a result, 3-bptzb adopts two types of conformations and acts as a tetradentate ligand with two pyridyl N atoms and two tetrazolyl atoms to connect the Ag^I ions, constructing a *meso*-helix chain. The adjacent *meso*-helix chains are further extended by Ag^I ions into a 3D MOF with large channels in which the PMo$_{12}$ anions reside. Construction of **2** proves the rationality of the synthetic strategy. In order to further confirm the rationality, we tried to explore another P$_2$W$_{18}$-based system also using the 3-bptzb ligand. Fortunately, a loop connecting loop chain is formed in **3**, which further proves the important role of the side N donor in the pyridyl group in construction of helix/loop structures. The loop connecting loop chains are connected by P$_2$W$_{18}$ anions to form 2D networks, which are further linked by the 3-bptzb ligand to construct a 3D framework. The 3-bptzb ligands exhibit three types of coordination modes with tetrazolyl and pyridyl groups in **3**. Finally, isomers of the 4- and 3-bptzb ligands exhibit key influences on construction of three compounds with helix/loop structures or not (Scheme 2).

Influences of POMs on the Structures of the Compounds. It is well known that the POMs play an important role in the assembly process of the POM-based MOCs and can induce structural diversities owing to their different charge and volume.[25] In this work, we obtained two distinct structures **2** and **3** both based on the Ag−3-bptzb system in which compound **2** contains Keggin PMo$_{12}$ anions and compound **3** has Wells-Dawson P$_2$W$_{18}$ anions. Compound **2** shows a 3D MOF constructed by Ag^I ions and 3-bptzb ligands with large channels. The PMo$_{12}$ anions offer two terminal O atoms to coordinate with two Ag2 atoms from the MOF and residing in the large channels, while in compound **3** the P$_2$W$_{18}$ anions act as five-connected inorganic ligands linking the adjacent loop connecting loop chains to construct hamburger-like 2D layers, which are further extended by 3-bptzb ligands into a 3D framework. In this 3D architecture the P$_2$W$_{18}$ anions are necessary components, which is different from the PMo$_{12}$ anions in **2**. This result indicates that the POMs anions with different volumes and charges play an important role in constructing novel and various frameworks.

FT-IR Spectra, XPS Spectra, PXRD, and TG Analyses. IR spectra of compounds **1**−**3** are shown in Figure S11, Supporting Information. Characteristic bands at 1063, 959, 877, and 801 cm^{-1} for **1** and 1058, 957, 872, and 799 cm^{-1} for **2** are attributed to ν(P−O), ν(Mo−O$_d$), and ν(Mo−O$_{b/c}$−Mo) of PMo$_{12}$.[26] Characteristic bands at 1095, 957, 912, and 789 cm^{-1} for **3** are the characteristic peaks of ν(P−O$_a$), ν(W−O$_d$), and ν(W−O$_{b/c}$−W) of P$_2$W$_{18}$.[27] Furthermore, the characteristic absorption bands at 1404 cm^{-1} for **1**, 1386 cm^{-1} for **2**, and 1363 cm^{-1} for **3** are attributed to ν(N=N) of the tetrazolyl ring of 4-bptzb and 3-bptzb ligands.[28] Characteristic bands at 1459, 1605, and 1645 cm^{-1} for **1**, 1451, 1561, and 1619 cm^{-1} for **2**, and 1466, 1584, and 1642 cm^{-1} for **3** are attributed to ν(C−C) and ν(C−N) of the pyridyl ring.[29] XPS spectra of compound **2** show two overlapped peaks at 232.5 and 231.5 eV attributed to Mo$_{3d}$$^{6+}$ and Mo$_{3d}$$^{5+}$, respectively (Figure S12, Supporting Information). This result is consistent with the valence sum calculations of **2** that one Mo atom of each PMo$_{12}$ anion is in the +V oxidation state. For compounds **1**−**3** and **2a** PXRD patterns are presented in Figure S13, Supporting Information. Both simulated and experimental patterns match

Scheme 2. Schematic Illustrations of the POMs-Based MOCs 1−3 Containing Different Ag−bptzb Subunits

Compound 1   Compound 2   Compound 3
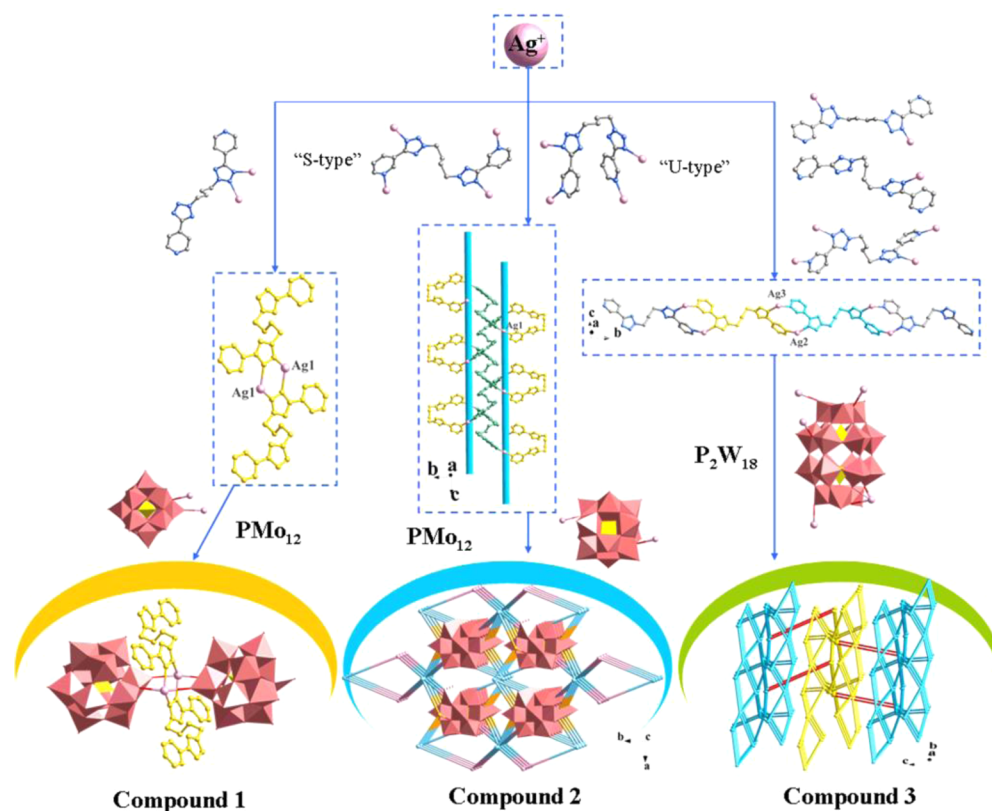
well, which indicate the good phase purities of compounds 1−3 and 2a. As shown in Figure S14, Supporting Information, the thermal stabilities of compounds 1−3 were investigated under a N₂ atmosphere with a heating rate of 10 °C·min⁻¹ in the temperature range of 20−800 °C. The TG curves of 1−3 exhibit a two-step weight loss process: the first weight loss of 2.4% (calcd 2.5%) for **1**, 1.5% (calcd 1.2%) for **2**, and 1.83% (calcd 1.6%) for **3** below 300 °C correspond to release of water molecules. After 300 °C, the second weight loss step can be ascribed as the loss of ligands 20.57% (calcd 20.73%) for **1**, 23.1% (calcd 23.3%) for **2**, and 15.18% (calcd 15.54%) for **3**.

Fluorescence Property. It is well known that metal−organic complexes with a d¹⁰ metal center usually show promising photoluminescent properties.[30] In this work, the fluorescent properties of the title compounds together with the free 4-bptzb and 3-bptzb ligands were studied in the solid state at room temperature. Emission spectra of the title compounds and free ligands are shown in Figure 8. It can be clearly seen that the free ligands exhibit emission peaks at 456 nm for 3-bptzb and 519 nm for 4-bptzb with excitation at 350 nm, which can probably be assigned to the intraligand π−π* transitions.[31] In contrast, the emission peaks at about 408 nm for **1**, 402 nm for **2**, and 405 nm for **3** are observed when they are excited at 310 nm. Compared with free bptzb ligands, the significant blue shift of emission peaks for the title compounds may be due to the ligands coordinating with Ag^I ions and then increasing the HOMO−LUMO energy levels of the title compounds.[20a,32]

In order to further explore the influence of guest molecules on the photoluminescent properties, fluorescent spectra of powder samples of **2a** (the guest-free form of **2**) were recorded. Desolvated **2a** samples were prepared as follows: samples **2** were immersed in CH₃OH for 3 days. Then the solvent-
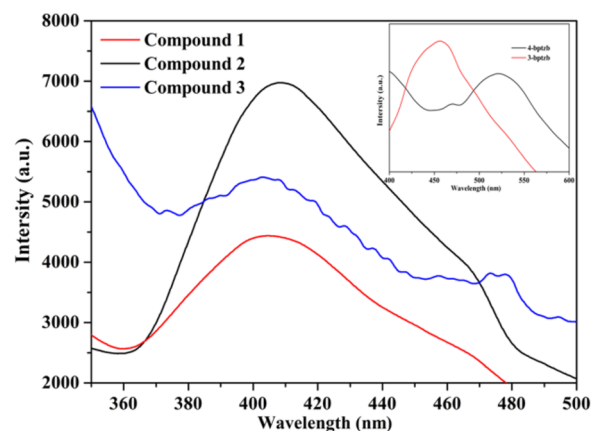
Figure 8. Emission spectra of compounds 1−3 and the bptzb (4-bptz and 3-bptzb) ligands (insert).

exchanged samples were evacuated at 60 °C for 1 h and 120 °C for over 3 h. It is noted that the fluorescent spectrum of **2a** shows fluorescent enhancement (Figure S15, Supporting Information), which indicates that the guest water molecules in **2** have an influence on the fluorescent intensity. In order to further confirm the influence of guest molecules on fluorescence intensity, the solid-state fluorescent properties of **2a** containing three aromatic molecules (designated as **2a**-aromatic molecules) have been investigated at room temperature. **2a**-aromatic molecules were prepared by immersing **2a** powder (5.0 mg) in 5.0 mL of methylbenzene, benzene, and nitrobenzene. After sonication treatment, aging for over 24 h, shaking, and filtering, **2a**-methylbenzene, **2a**-benzene, and **2a**-nitrobenzene were obtained after drying in air. As shown in

Figure S16, Supporting Information, nitrobenzene enhances the emission intensity of **2a**. However, benzene and methylbenzene are a fluorescence quencher for **2a**. The results demonstrate that **2a** may be regarded as a potential fluorescence sensor to detect some aromatic molecules.

Voltammetric Behavior of 2−CPE and 3−CPE and Their Parent POMs in Aqueous Solution and Their Electrocatalytic Activitiy. The bulk-modified carbon paste electrodes (CPEs) with POM-based MOCs have been widely applied in electrochemistry due to their advantages: high stability, low solubility in water and common organic solvents, easy to handle and prepare, and so on.[33] Thus, the electrochemical activities of **2** and **3** were explored using **2**−CPE and **3**−CPE in this work. As shown in Figure 9, the cyclic
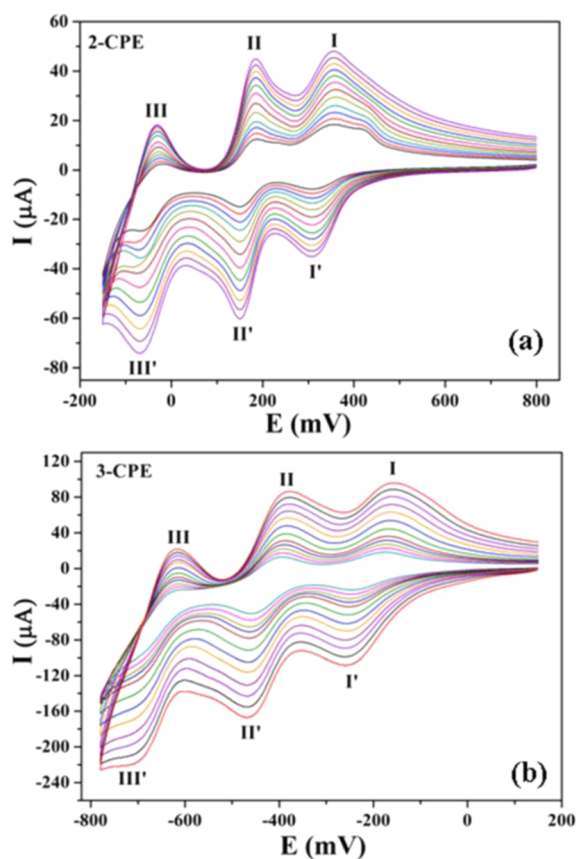
Figure 9. Cyclic voltammograms of the **2**−CPE (a) and **3**−CPE (b) in 0.1 M H_2SO_4 + 0.5 M Na_2SO_4 aqueous solution at different scan rates (from inner to outer: 60, 80, 100, 120, 160, 200, 250, 300, 350, 400, 450, and 500 mV·s^{-1}).

voltammograms for the **2**−CPE and **3**−CPE in 0.1 M H_2SO_4 + 0.5 M Na_2SO_4 aqueous solution at different scan rates are presented. In the potential range from +800 to −150 mV, three reversible redox peaks (I−I′, II−II′, III−III′) appear with the mean peak potentials $E_{1/2} = (E_{pa} + E_{pc})/2$ (scan rate 100 mV·s^{-1}) of +335 (I−I′), +167 (II−II′), and −49 (III−III′) mV for **2**−CPE, which correspond to three consecutive two-electron processes of Mo centers of PMo_{12}.[34] In the potential range from +150 to −780 mV for **3**−CPE (Figure 9b), there exist three reversible redox peaks with the mean peak potentials of −206 (I−I′), −425 (II−II′), and −663 (III−III′) mV (scan rate 100 mV·s^{-1}), which correspond to three consecutive two-electron processes of the W centers of P_2W_{18}.[35] Furthermore,

with the scan rates increasing the peak potentials of cyclic voltammograms for the two bulk-modified CPEs change gradually: the cathodic peak potentials shift toward the negative direction and the corresponding anodic peak potentials to the positive direction. Peak currents are proportional to the scan rates up to 500 mV·s^{-1} (Figure S17, Supporting Information), which indicate the redox process of the **2**−CPE and **3**−CPE is surface controlled.[36]

The electrochemical behavior of the parent POMs was also investigated using PMo_{12}−CPE and P_2W_{18}−CPE as the working electrodes in the same conditions, as shown in Figure S18, Supporting Information. Comparing with the **2**−CPE, the cyclic voltammogram for the PMo_{12}−CPE in 0.1 M H_2SO_4 + 0.5 M Na_2SO_4 aqueous solution at different scan rates is similar to that of **2**−CPE except for the different mean peak potentials of three reversible redox peaks (I−I′, II−II′, and III−III′). The same observation is obtained in the comparison of **3**−CPE and P_2W_{18}−CPE. These results indicate that the redox abilities of the parent PMo_{12} and P_2W_{18} polyoxoanions could be maintained in the hybrid solids, which promises an application of this kind of inorganic−organic hybrid materials in electrochemistry. Furthermore, compared with the PMo_{12}−CPE and P_2W_{18}−CPE, the slight potential shifts of the three redox peaks in **2**−CPE and **3**−CPE may be related to the combination with Ag−(3-bptzb) complex cations.

As is known, some POMs can be used as electrocatalysts to catalyze the reduction of nitrite and hydrogen peroxide, etc.[37] In this work, we first investigated the electrocatalytic activities of **2**− and **3**−CPEs on the reductions of nitrite and hydrogen peroxide. Figure 10 shows cyclic voltammograms for the electrocatalytic reduction of nitrite at **2**− and **3**−CPEs in 0.1 M H_2SO_4 + 0.5 M Na_2SO_4 aqueous solution. It can be seen that, with addition of nitrite, the reduction peak currents gradually increase and corresponding oxidation peak currents decrease, which indicates that the three reduced species of the polyoxoanions show good electrocatalytic activity toward the reduction of nitrite. Figure S19, Supporting Information, shows cyclic voltammograms for the electrocatalytic reduction of hydrogen peroxide at **2**− and **3**−CPEs. For the **2**−CPE, with addition of hydrogen peroxide, only the third reduction peak current increases gradually while the corresponding oxidation peak current gradually decreases. However, the first and second peaks remain almost unchanged, indicating that only the six-electron-reduced species of PMo_{12} anion have electrocatalytic activity for reduction of hydrogen peroxide. For the **3**−CPE, with addition of hydrogen peroxide, the second and third reduction peak currents increase gradually while the corresponding oxidation peak currents gradually decrease. However, the first peak remains almost unchanged, indicating that the four- and six-electron-reduced species of P_2W_{18} anions possess electrocatalytic activity for reduction of hydrogen peroxide. In addition, we also investigated the electrocatalytic activities of PMo_{12}−CPE and P_2W_{18}−CPE on the reductions of nitrite and hydrogen peroxide (Figures S20 and S21, Supporting Information). The results indicate that the electrocatalytic activities toward the reduction of nitrite and hydrogen peroxide of the parent PMo_{12} and P_2W_{18} polyoxoanions could be maintained in the hybrid solids.
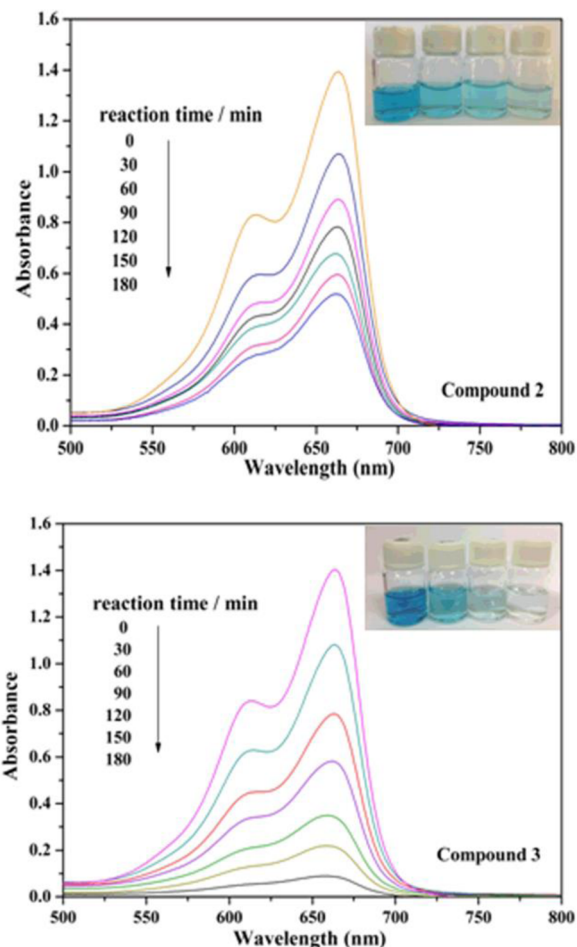
Photocatalytic Activity. Photocatalytic degeneration of organic dyes is one of the effective methods to eliminate pollutants.[38] To investigate the photocatalytic activities of compounds **2** and **3** as catalysts, photodecomposition of methylene blue (MB), rhodamine B (RhB), and methyl orange
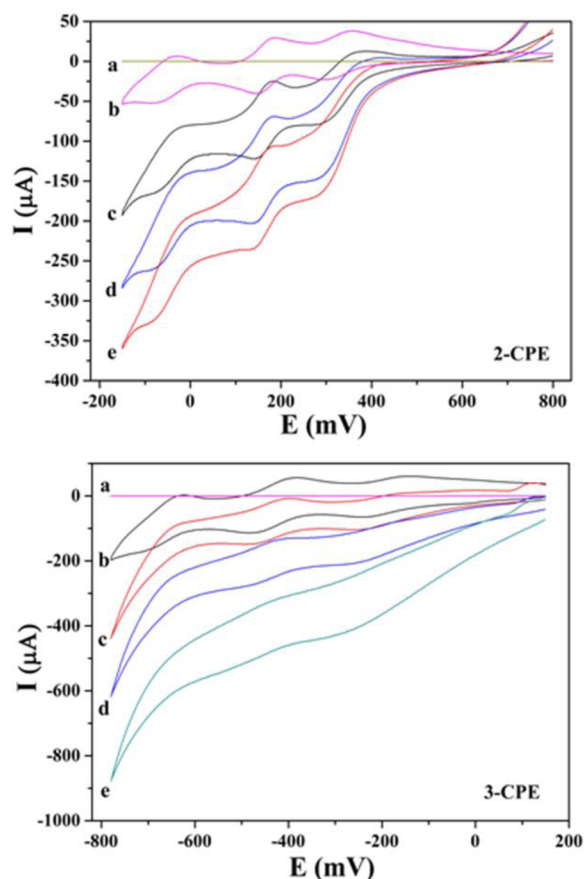
Figure 10. Cyclic voltammograms of the **2**−CPE and **3**−CPE in 0.1 M H$_2$SO$_4$ + 0.5 M Na$_2$SO$_4$ aqueous solution containing 0 (b), 2(c), 4 (d), and 6 (e) mM NaNO$_2$ and a bare CPE (a) in a 6.0 mM NaNO$_2$ + 0.1 M H$_2$SO$_4$ + 0.5 M Na$_2$SO$_4$ solution. Scan rate: 200 mV·s^{-1}.

Figure 11. Absorption spectra of the MB solution during the decomposition reaction under UV irradiation with the presence of compounds **2** and **3**.

(MO) solution as model organic pollutants was carried out under UV irradiation from a 125 W Hg lamp. In the process of photocatalysis, 100 mg of compound **2** or **3** was mixed in 0.02 mmol/L aqueous solution of organic dyes (MB/RhB/MO) 250 mL and magnetically stirred for about 10 min until equilibrium of the mixture. Then, every 30 min, 3.0 mL samples were taken out for analysis by UV−vis spectroscopy. As shown in Figure 11, the absorption peaks of MB were gradually reduced with time, increasing from 0 to 180 min. After 180 min, the degradation ratio of MB reaches 63% for **2** and 94% for **3** (Figure S22, Supporting Information). The results indicate that compounds **2** and **3** have good photocatalytic activity for degradation of MB in aqueous solution. In particular, compound **3** shows very high photocatalytic efficiency for degradation of MB in aqueous solution. Similar procedures were performed to investigate the photocatalytic activities of compounds **2** and **3** on degradation of RhB and MO. In comparison, the absorption peaks of RhB and MO show no obvious change after 180 min (Figure S23, Supporting Information).

Photodegradation of MB, RhB, and MO catalyzed by parent POMs was performed under the same conditions in order to compare with title compounds (Figure S24, Supporting Information). After 180 min, the degradation ratio of MB is 42% for PMo$_{12}$ and 49% for P$_2$W$_{18}$ (Figure S25a, Supporting Information), which is lower than that of **2** and **3** as catalysts, respectively, namely, the POM−Ag−bptzb systems can

improve the photocatalytic activity of parent POMs toward degradation of MB. However, the degradation ratio of RhB catalyzed by parent POMs reaches 62% for PMo$_{12}$ and 55% for P$_2$W$_{18}$ in 180 min (Figure S25b, Supporting Information), which is higher than that of **2** and **3**. The absorption peaks of MO also show no obvious change in the presence of PMo$_{12}$ and P$_2$W$_{18}$. The difference of title compounds and parent POMs for their photocatalysis activity toward degradation of MB and RhB may be attributed to O−Mo/W charge transfer.[39] The results indicate that compounds **2** and **3** show photocatalytic selectivity for the degradation of organic dyes, especially for degradation of MB with higher ratio.

■ CONCLUSION

Using two unprecedented flexible bis(pyridyl-tetrazole) ligands 4- and 3-bptzb and Ag^I ions as building elements to modify two types of POM anions, three POM-based MOCs with different Ag−bptzb subunits were successfully obtained. The syntheses of compounds **2** and **3** confirm that the side N donors in the pyridyl group of 3-bptzb are conducive to forming helix/loop subunits. The POMs anions exhibit great influences on the construction of various architectures. Compound **3** shows excellent photocatalytic activity and selectivity for degradation of organic dyes, which may be used as a potential and valuable photocatalyst. Successful isolation of these solid materials convinced us that targeted syntheses of POM-based MOCs can

be realized by the design of proper organic ligands. Further study on some other ligands with side coordination donors to construct helix/loop structures is underway.

■ ASSOCIATED CONTENT

Ⓢ Supporting Information

X-ray crystallographic data in CIF format, selected bond lengths and angles, structure illustrations for compounds **1**−**3**, FT-IR spectra, PXRD, and TG analyses of compounds **1**−**3**, voltammetric curves and photocatalytic properties for compounds **2** and **3**. This material is available free of charge via the Internet at http://pubs.acs.org.

■ AUTHOR INFORMATION

Corresponding Author
*Phone: +86-416-3400158. E-mail: wangxiuli@bhu.edu.cn.
Notes
The authors declare no competing financial interest.

■ ACKNOWLEDGMENTS

■ REFERENCES

(1) (a) Cui, P.; Ma, Y. G.; Li, H. H.; Zhao, B.; Li, J. R.; Cheng, P.; Balbuena, P. B.; Zhou, H. C. *J. Am. Chem. Soc.* **2012**, *134*, 18892. (b) Guo, H. L.; Zhu, G. S.; Hewitt, I. J.; Qiu, S. L. *J. Am. Chem. Soc.* **2009**, *131*, 1646. (c) Deria, P.; Mondloch, J. E.; Tylianakis, E.; Ghosh, P.; Bury, W.; Snurr, R. Q.; Hupp, J. T.; Farha, O. K. *J. Am. Chem. Soc.* **2013**, *135*, 16801.

(2) (a) Bisht, K. K.; Suresh, E. *J. Am. Chem. Soc.* **2013**, *135*, 15690. (b) Zhou, X. P.; Wu, Y.; Li, D. *J. Am. Chem. Soc.* **2013**, *135*, 16062. (c) Li, X. X.; Xu, H. Y.; Kong, F. Z.; Wang, R. H. *Angew. Chem., Int. Ed.* **2013**, *52*, 1. (d) Tian, D.; Chen, Q.; Li, Y.; Zhang, Y. H.; Chang, Z.; Bu, X. H. *Angew. Chem., Int. Ed.* **2014**, *53*, 537.

(3) (a) Yaghi, O. M.; Li, H. L. *J. Am. Chem. Soc.* **1996**, *118*, 295. (b) Vilar, R.; Mingos, D. M. P.; White, A. J. P.; Williams, D. J. *Angew. Chem., Int. Ed.* **1998**, *37*, 9. (c) Cheetham, A. K.; Ferey, G.; Loiseau, T. *Angew. Chem., Int. Ed.* **1999**, *38*, 3268. (d) Tabares, L. C.; Navarro, J. A. R.; Salas, J. M. *J. Am. Chem. Soc.* **2001**, *123*, 383.

(4) (a) Wu, C. D.; Lu, C. Z.; Zhuang, H. H.; Huang, J. S. *J. Am. Chem. Soc.* **2002**, *124*, 3836. (b) Oliva, A. R. D. L.; Sans, V.; Miras, H. N.; Yan, J.; Zang, H. Y.; Richmond, C. J.; Long, D. L.; Cronin, L. *Angew. Chem., Int. Ed.* **2012**, *51*, 1. (c) Miras, H. N.; Sorus, M.; Hawkett, J.; Sells, D. O.; McInnes, E. J. L.; Cronin, L. *J. Am. Chem. Soc.* **2012**, *134*, 6980. (d) Gao, G. G.; Cheng, P. S.; Mak, T. C. W. *J. Am. Chem. Soc.* **2009**, *131*, 18257. (e) Zhang, J.; Hao, J.; Wei, Y. G.; Xiao, F. P.; Yin, P. C.; Wang, L. S. *J. Am. Chem. Soc.* **2010**, *132*, 14. (f) Huang, P.; Qin, C.; Su, Z. M.; Xing, Y.; Wang, X. L.; Shao, K. Z.; Lan, Y. Q.; Wang, E. B. *J. Am. Chem. Soc.* **2012**, *134*, 14004. (g) Haralampos, N. M.; Yan, J.; Long, D. L.; Cronin, L. *Chem. Soc. Rev.* **2012**, *41*, 7403. (h) Dolbecq, A.; Dumas, E.; Mayer, C. R.; Mialane, P. *Chem. Rev.* **2010**, *110*, 6009. (i) Gouzerh, P.; Proust, A. *Chem. Rev.* **1998**, *98*, 77. (j) Kozhevnikov, I. V. *Chem. Rev.* **1998**, *98*, 171.

(5) (a) Wang, X. L.; Qin, C.; Wang, E. B.; Su, Z. M.; Li, Y. G.; Xu, L. *Angew. Chem., Int. Ed.* **2006**, *45*, 7411. (b) Ma, F. J.; Liu, S. X.; Sun, C. Y.; Liang, D. D.; Ren, G. J.; Wei, F.; Chen, Y. G.; Su, Z. M. *J. Am. Chem. Soc.* **2011**, *133*, 4178. (c) Fu, H.; Qin, C.; Lu, Y.; Zhang, Z. M.; Li, Y. G.; Su, Z. M.; Li, W. L.; Wang, E. B. *Angew. Chem., Int. Ed.* **2012**, *51*, 7985. (d) Meng, X.; Qin, C.; Wang, X. L.; Su, Z. M.; Li, B.; Yang, Q. H. *Dalton Trans.* **2011**, *40*, 9964. (e) Du, D. Y.; Qin, J. S.; Li, S. L.;

Su, Z. M.; Lan, Y. Q. *Chem. Soc. Rev.* **2014**, *43*, 4615. (f) Coronado, E.; Gómez-García, C. J. *Chem. Rev.* **1998**, *98*, 273.

(6) (a) Dolbecq, A.; Mialane, P.; Secheresse, F.; Keita, B.; Nadjo, L.; Rodriguez-Albelo, L. M.; Ruiz-Salvador, A. R.; Sampieri, A.; Lewis, D. W.; Gomez, A.; Nohra, B.; Mialane, P.; Marrot, J.; Secheresse, F.; Mellot-Draznieks, C.; Biboum, R. N.; Keita, B.; Nadjo, L.; Dolbecq, A. *J. Am. Chem. Soc.* **2009**, *131*, 16078. (b) Nohra, B.; Moll, H. E.; Rodriguez-Albelo, L. M.; Mialane, P.; Marrot, J.; Draznieks, C. M.; O'Keeffe, M.; Biboum, R. N.; Lemaire, J.; Keita, B.; Nadjo, L.; Dolbecq, A. *J. Am. Chem. Soc.* **2011**, *133*, 13363. (c) Liu, D.; Lu, Y.; Tan, H. Q.; Chen, W. L.; Zhang, Z. M.; Li, Y. G.; Wang, E. B. *Chem. Commun.* **2013**, *49*, 3673. (d) Wang, X. L.; Hu, H. L.; Liu, G. C.; Lin, H. Y.; Tian, A. X. *Chem. Commun.* **2010**, *46*, 6485. (e) Zheng, S. T.; Zhang, J.; Li, X. X.; Fang, W. H.; Yang, G. Y. *J. Am. Chem. Soc.* **2010**, *132*, 15102.

(7) (a) Liu, B.; Yang, J.; Yang, G. C.; Ma, J. F. *Inorg. Chem.* **2013**, *52*, 84. (b) Sha, J. Q.; Li, M. T.; Sun, J. W.; Yan, P. F.; Li, G. M.; Zhang, L. *Chem.—Asian J.* **2013**, *8*, 2254. (c) Zhu, M.; Su, S. Q.; Song, X. Z.; Hao, Z. M.; Song, S. Y.; Zhang, H. J. *CrystEngComm* **2012**, *14*, 6452. (d) Sha, J. W.; Li, M. T.; Sha, J. Q.; Yan, P. F.; Wang, C.; Li, S. X.; Pan, Y. *CrystEngComm* **2013**, *15*, 10584.

(8) (a) Wang, X. L.; Xu, C.; Lin, H. Y.; Liu, G. C.; Yang, S.; Gao, Q.; Tian, A. X. *CrystEngComm* **2012**, *14*, 5836. (b) Tian, A. X.; Ying, J.; Peng, J.; Sha, J. Q.; Pang, H. J.; Zhang, P. P.; Chen, Y.; Zhu, M.; Su, Z. M. *Inorg. Chem.* **2009**, *48*, 100.

(9) (a) Kan, W. Q.; Ma, J. F.; Liu, Y. Y.; Wu, H.; Yang, J. *CrystEngComm* **2011**, *13*, 7037. (b) Hou, G. F.; Bi, L. H.; Li, B.; Wu, L. X. *Inorg. Chem.* **2010**, *49*, 6474. (c) Lan, Y. Q.; Li, S. L.; Wang, X. L.; Shao, K. Z.; Du, D. Y.; Zang, H. Y.; Su, Z. M. *Inorg. Chem.* **2008**, *47*, 8187. (d) Dong, B. X.; Peng, J.; Gómez-García, C. J.; Benmansour, S.; Jia, H. Q.; Hu, N. H. *Inorg. Chem.* **2007**, *43*, 5933.

(10) (a) Liu, B.; Yu, Z. T.; Yang, J.; Hua, W.; Liu, Y. Y.; Ma, J. F. *Inorg. Chem.* **2011**, *50*, 8967. (b) Kan, W. Q.; Yang, J.; Liu, Y. Y.; Ma, J. F. *Inorg. Chem.* **2012**, *51*, 11266. (c) Tian, A. X.; Yang, Y.; Ying, J.; Li, N.; Lin, X. L.; Zhang, J. W.; Wang, X. L. *Dalton Trans.* **2014**, *43*, 8405.

(11) Ren, Y. P.; Kong, X. J.; Long, L. S.; Huang, R. B.; Zheng, L. S. *Cryst. Growth Des.* **2006**, *6*, 572.

(12) (a) Wang, X. L.; Wang, Y. F.; Liu, G. C.; Tian, A. X. *Dalton Trans.* **2011**, *40*, 9299. (b) Tian, A. X.; Lin, X. L.; Ying, J.; Zhang, J. W.; Lin, H. Y.; Liu, G. C.; Zhao, D.; Li, N.; Wang, X. L. *Dalton Trans.* **2013**, *42*, 9809. (c) Wang, X. L.; Li, N.; Tian, A. X.; Ying, J.; Liu, G. C.; Lin, H. Y.; Zhang, J. W.; Yang, Y. *Dalton Trans.* **2013**, *42*, 14856.

(13) Sheldrick G. M. *SHELXS-97*; University of Göttingen: Germany, 1997.

(14) Wang, X. L.; Kang, Z. H.; Wang, E. B.; Hu, C. W. *Mater. Lett.* **2002**, *56*, 393.

(15) Wang, X. L.; Zhao, D.; Tian, A. X.; Ying, J. *CrystEngComm* **2013**, *15*, 4516.

(16) Brown, I. D.; Altermatt, D. *Acta Crystallogr., Sect. B* **1985**, *41*, 244.

(17) Wang, X. L.; Li, J.; Tian, A. X.; Zhao, D.; Liu, G. C.; Lin, H. Y. *Cryst. Growth Des.* **2011**, *11*, 3456.

(18) Bai, Y.; Zhang, G. Q.; Dang, D. B.; Ma, P. T.; Gao, H.; Niu, J. Y. *CrystEngComm* **2013**, *15*, 4516.

(19) (a) Yang, M. X.; Lin, S.; Chen, L. J.; Zhang, X. F.; Huang, H. *Inorg. Chem. Commun.* **2011**, *14*, 1652. (b) Dong, P.; Zhang, Q. K.; Wang, F.; Chen, S. C.; Wu, X. Y.; Zhao, Z. G.; Lu, C. Z. *Cryst. Growth Des.* **2010**, *10*, 3218. (c) Wu, X. Y.; Dong, P.; Yu, R. M.; Zhang, Q. K.; Kuang, X. F.; Chen, S. C.; Lin, Q. P.; Lu, C. Z. *CrystEngComm* **2011**, *13*, 368. (d) Darling, K.; Smith, T. M.; Vargas, J.; O'Connor, C. J.; Zubieta, J. *Inorg. Chem. Commun.* **2013**, *32*, 1.

(20) (a) Sha, J. Q.; Sun, J. W.; Wang, C.; Li, G. M.; Yan, P. F.; Li, M. T.; Liu, M. Y. *CrystEngComm* **2012**, *14*, 5053. (b) Sha, J. Q.; Liang, L. Y.; Sun, J. W.; Tian, A. X.; Yan, P. F.; Li, G. M.; Wang, C. *Cryst. Growth Des.* **2012**, *12*, 894.

(21) Liu, M. G.; Zhang, P. P.; Peng, J.; Meng, H. X.; Wang, X.; Zhu, M.; Wang, D. D.; Meng, C. L.; Alimaje, K. *Cryst. Growth Des.* **2012**, *12*, 1273.

(22) (a) Liu, C. M.; Zhang, D. Q.; Zhu, D. B. *Cryst. Growth Des.* **2006**, *6*, 524. (b) Zang, H. Y.; Lan, Y. Q.; Yang, G. S.; Wang, X. L.; Shao, K. Z.; Xu, G. J.; Su, Z. M. *CrystEngComm* **2010**, *12*, 434. (c) Qi, Y. F.; Wang, E. B.; Li, J.; Li, Y. G. *J. Solid State Chem.* **2009**, *182*, 2640. (d) Sha, J. Q.; Li, M. T.; Sun, J. W.; Zhang, Y. N.; Yan, P. F.; Li, G. M. *Dalton Trans.* **2013**, *42*, 7803.

(23) (a) Lu, Y.; Xu, Y.; Wang, E. B.; Lü, J.; Hu, C. W.; Xu, L. *Cryst. Growth Des.* **2005**, *5*, 257. (b) Zheng, P. Q.; Ren, Y. P.; Long, L. S.; Huang, R. B.; Zheng, L. S. *Inorg. Chem.* **2005**, *44*, 1190. (c) Jin, H.; Qi, Y. F.; Wang, E. B.; Li, Y. G.; Wang, X. L.; Qin, C.; Chang, S. *Cryst. Growth Des.* **2006**, *6*, 2693.

(24) (a) Du, X. D.; Li, C. H.; Zhang, Y.; Liu, S.; Ma, Y.; You, X. Z. *CrystEngComm* **2011**, *13*, 2350. (b) Kan, W. Q.; Ma, J. F.; Liu, Y. Y.; Wu, H.; Yang, J. *CrystEngComm* **2011**, *13*, 7037. (c) Zhang, C. J.; Pang, H. J.; Tang, Q.; Wang, H. Y.; Chen, Y. G. *New J. Chem.* **2011**, *35*, 190. (d) Gong, J. J.; Zhang, W. S.; Liu, Y.; Zhang, H. C.; Hu, H. L.; Kang, Z. H. *Dalton Trans.* **2012**, *41*, 5468.

(25) Zhu, M.; Su, S. Q.; Song, X. Z.; Hao, Z. M.; Song, S. Y.; Zhang, H. J. *CrystEngComm* **2012**, *14*, 6452.

(26) Liu, H. Y.; Wu, H.; Yang, J.; Liu, Y. Y.; Ma, J. F.; Bai, H. Y. *Cryst. Growth Des.* **2011**, *11*, 1786.

(27) Tian, A. X.; Ying, J.; Peng, J.; Sha, J. Q.; Han, Z. G.; Ma, J. F.; Su, Z. M.; Hu, N. H.; Jia, H. Q. *Inorg. Chem.* **2008**, *47*, 3274.

(28) Goswami, S.; Sanda, S.; Konar, S. *CrystEngComm* **2014**, *16*, 369.

(29) Reinoso, S.; Vitoria, P.; Felices, L. S.; Montero, A.; Lezama, L.; Gutiérrez-Zorrilla, J. M. *Inorg. Chem.* **2007**, *46*, 1237.

(30) (a) Wang, X. L.; Chen, Y. Q.; Gao, Q.; Lin, H. Y.; Liu, G. C.; Zhang, J. X.; Tian, A. X. *Cryst. Growth. Des.* **2010**, *10*, 2174. (b) Lan, Y. Q.; Li, S. L.; Wang, X. L.; Shao, K. Z.; Du, D. Y.; Zang, H. Y.; Su, Z. M. *Inorg. Chem.* **2008**, *47*, 8179. (c) Zhang, J. P.; Lin, Y. Y.; Huang, X. C.; Chen, X. M. *J. Am. Chem. Soc.* **2005**, *127*, 5492. (d) Liu, C. S.; Chen, P. Q.; Chang, Z.; Wang, J. J.; Yan, L. F.; Sun, H. W.; Bu, X. H.; Lin, Z. Y.; Li, Z. M.; Batten, S. R. *Inorg. Chem. Commun.* **2008**, *11*, 159.

(31) Wang, X.; Peng, J.; Liu, M. G.; Wang, D. D.; Meng, C. L.; Li, Y.; Shi, Z. Y. *CrystEngComm* **2012**, *14*, 3220.

(32) (a) Shi, X.; Zhu, G.; Fang, Q.; Wu, G.; Tian, G.; Wang, R.; Zhang, D.; Xue, M.; Qiu, S. *Eur. J. Inorg. Chem.* **2004**, *1*, 185. (b) Zhang, X. M.; Tong, M. L.; Gong, M. L.; Chen, X. M. *Eur. J. Inorg. Chem.* **2003**, *1*, 138.

(33) (a) Sadakane, M.; Steckhan, E. *Chem. Rev.* **1998**, *98*, 219. (b) Jiang, Z. G.; Shi, K.; Lin, Y. W.; Wang, Q. M. *Chem. Commun.* **2014**, *50*, 2353. (c) Zhang, Y.; Shen, J. Q.; Zheng, L. H.; Zhang, Z. M.; Li, Y. X.; Wang, E. B. *Cryst. Growth Des.* **2014**, *14*, 110.

(34) Hao, X. L.; Ma, Y. Y.; Zhang, C.; Wang, Q.; Cheng, X.; Wang, Y. H.; Li, Y. G.; Wang, E. B. *CrystEngComm* **2012**, *14*, 6573.

(35) (a) Xi, X. D.; Dong, S. J. *J. Mol. Catal. A: Chem.* **1996**, *114*, 257. (b) McCormac, T.; Fabre, B.; Bidan, G. *J. Electroanal. Chem.* **1997**, *425*, 49.

(36) Sha, J. Q.; Peng, J.; Lan, Y. Q.; Su, Z. M.; Pang, H. J.; Tian, A. X.; Zhang, P. P.; Zhu, M. *Inorg. Chem.* **2008**, *47*, 5145.

(37) (a) Toth, J. E.; Anson, F. C. *J. Am. Chem. Soc.* **1989**, *111*, 2444. (b) Dong, S. J.; Xi, X. D.; Tian, M. *J. Electroanal. Chem.* **1995**, *385*, 227. (c) Keita, B.; Belhouari, A.; Nadjo, L.; Contant, R. *J. Electroanal. Chem.* **1995**, *381*, 243. (d) Toth, J. E.; Anson, F. C. *J. Electroanal. Chem.* **1988**, *256*, 361.

(38) (a) Hu, Y.; Luo, F.; Dong, F. F. *Chem. Commun.* **2011**, *47*, 761. (b) Chen, Y. Q.; Liu, S. J.; Li, Y. W.; Li, G. R.; He, K. H.; Qu, Y. K.; Hu, T. L.; Bu, X. H. *Cryst. Growth Des.* **2012**, *12*, 5426. (c) Pang, H. J.; Ma, H. Y.; Peng, J.; Zhang, C. J.; Zhang, P. P.; Su, Z. M. *CrystEngComm* **2011**, *13*, 7079.

(39) (a) Li, T. H.; Gao, S. Y.; Li, F.; Cao, R. *J. Colloid Interface Sci.* **2009**, *338*, 500. (b) Dolbecq, A.; Mialane, P.; Keita, B.; Nadjo, L. *J. Mater. Chem.* **2012**, *22*, 24509.